

Faraday Discussions

Accepted Manuscript



This manuscript will be presented and discussed at a forthcoming Faraday Discussion meeting. All delegates can contribute to the discussion which will be included in the final volume.

Register now to attend! Full details of all upcoming meetings: <http://rsc.li/fd-upcoming-meetings>



This is an *Accepted Manuscript*, which has been through the Royal Society of Chemistry peer review process and has been accepted for publication.

Accepted Manuscripts are published online shortly after acceptance, before technical editing, formatting and proof reading. Using this free service, authors can make their results available to the community, in citable form, before we publish the edited article. We will replace this *Accepted Manuscript* with the edited and formatted *Advance Article* as soon as it is available.

You can find more information about *Accepted Manuscripts* in the [Information for Authors](#).

Please note that technical editing may introduce minor changes to the text and/or graphics, which may alter content. The journal's standard [Terms & Conditions](#) and the [Ethical guidelines](#) still apply. In no event shall the Royal Society of Chemistry be held responsible for any errors or omissions in this *Accepted Manuscript* or any consequences arising from the use of any information it contains.

ARTICLE

Oxide Diffusion in Innovative SOFC cathode materials

Cite this: DOI: 10.1039/x0xx00000x

Y. Hu^a, V. Thoréton^b, C. Pirovano^b, E. Capoen^b, C. Bogicevic^a, N. Nuns^b, A.-S. Mamede^b, G. Dezanneau^a and R. N. Vannier^{b*}Received 00th January 2012,
Accepted 00th January 2012

DOI: 10.1039/x0xx00000x

www.rsc.org/

Oxide diffusion was studied in two innovative SOFC cathode materials, Ba₂Co₉O₁₄ and Ca₃Co₄O_{9+δ} derivatives. Although oxygen diffusion was confirmed in the promising Ba₂Co₉O₁₄, it was not possible to derive accurate transport parameters because of an oxidation process at the sample surface which has still to be clarified. In contrast, the oxygen diffusion in the well-known Ca₃Co₄O_{9+δ} thermoelectric materials was improved when calcium was partly substituted with strontium, likely due to an increase of the volume of the rock salt layers in which the conduction process takes place. Although the diffusion coefficient remains low, interestingly, fast kinetics towards the oxygen molecule dissociation reaction were shown with surface exchange coefficients higher than those reported for the best cathode materials in the field. They increased with the strontium content, the Sr atoms potentially playing a key role in the mechanism of oxygen molecule dissociation at the solid surface.

Introduction

With the possibility of cogeneration of electricity and heat, Solid Oxide Fuel cells are promising. First units were commercialised in Japan in 2009 and demonstrators are running in Europe. Their principle is based on a dense ceramic electrolyte which separates two compartments, one containing hydrogen, and the other containing air. Because of a difference of oxygen chemical potential between the two compartments, oxygen molecules are reduced at the cathode into oxide ions, which migrate through the electrolyte to the anode to react with hydrogen molecule and produce water. Hydrogen is usually produced by methane reforming, however internal reforming of methane is also envisaged. Typical temperatures of use range are in between 700 and 1000°C. The main electrolyte materials which are currently studied are Yttria Stabilised Zirconia (YSZ), Gadolinia Doped Ceria (GDC) and lanthanum gallates (LSGM). At the anode, a Ni-YSZ cermet containing 40% in volume of nickel is usually developed, but it is prone to carbon deposition when used with hydrocarbon fuels. It is also sensitive to sulphur poisoning and suffer from nickel agglomeration and redox stability under prolonged usage. Alternative materials such as the chromo-manganites (La_{0.75}Sr_{0.25})Cr_{0.5}Mn_{0.5}O₃ or titanates such as lanthanum doped SrTiO₃ have been proposed. At the cathode, the strontium substituted lanthanum manganite (La_{1-x}Sr_xMnO_{3-δ}) is conventionally used. However, it displays low oxide ion conductivity and composites with YSZ were developed to allow its use at temperature lower than 800°C. To operate at lower

temperature, Mixed Ionic Electronic Conductors (MIEC) are usually preferred to allow the oxygen reduction reaction to be sprayed on the whole electrode volume and not only at the electrode/electrolyte interface. As an alternative to LSM, the La_{0.6}Sr_{0.4}Co_{0.2}Fe_{0.8}O_{3-δ} (LSCF) perovskite has been widely studied¹. When used with a GDC electrolyte and after optimisation of its microstructure, an area specific resistance (ASR) of only 0.13 Ω.cm² was obtained at 603°C for this compound², the target for the cathode being 0.15 Ω.cm² at 700°C. These high performances are likely due to the presence of Co(III) in the structure which is known to be particularly active for the reduction of oxygen molecules into oxide ions³. Indeed, cobaltites are known to display high oxide ion transport parameters. Among these, the La_{0.6}Sr_{0.4}CoO_{3-δ} composition is among the best catalyst for the oxygen molecule reduction reaction with a surface exchange coefficient (*k**, cm/s) of 1.1×10⁻⁶ cm/s associated to an oxygen self-diffusion tracer (*D**, cm²/s) coefficient of 2.0×10⁻⁸ cm²/s at 680°C under 230 mbar⁴. One drawback of these materials is their high thermal expansion coefficient with a value of 23×10⁻⁶ K⁻¹ for this later composition which is twice the thermal expansion of YSZ (10×10⁻⁶ K⁻¹)⁵ and GDC (12×10⁻⁶ K⁻¹)⁶. However, partial substitution of cobalt with iron in LSCF led to a good compromise with a TEC in the range of 14-15×10⁻⁶ K⁻¹ from 500 to 700°C⁷. More recently, promising performances as SOFC cathodes were shown for two innovative cobaltites, Ba₂Co₉O₁₄ and Ca₃Co₄O_{9+δ}. An ASR of 0.5 Ω.cm² was first measured on a symmetric cell made of a 70 wt% Ba₂Co₉O₁₄ - 30 wt% GDC composite electrode, deposited on a GDC

electrolyte⁸. The good electrochemical performances of this compound were later confirmed by Li *et al.* who obtained ASR of only 0.133 $\Omega\cdot\text{cm}^2$ and 0.068 $\Omega\cdot\text{cm}^2$ at 750 and 850 °C and powder density of 450 mW/cm² and 770 mW/cm² on a cell made of a LSGM electrolyte with a Ba₂Co₉O₁₄ – samarium doped ceria composite cathode at 800 and 850°C, respectively³. This compound exhibits a three dimension structure based on a [Co₈O₈] blocks sandwiched in between [Ba₂CoO₆] layers^{9,10} (Fig. 1a). With cobalt atoms at difference valences, it displays high electronic conductivity with a value of 240 S.cm⁻¹ at 650°C but as other cobaltites, its thermal expansion coefficient is high (22×10^{-6} K⁻¹) which supposes the use of a composite at least for mechanical compatibility between the electrode and the electrolyte. After optimisation of its composition and thickness, an ASR of only 0.08 $\Omega\cdot\text{cm}^2$ at 700°C was recently measured on symmetric cell made of a 50 wt% Ba₂Co₉O₁₄ – 50 wt% GDC composite electrode with a GDC electrolyte¹¹.

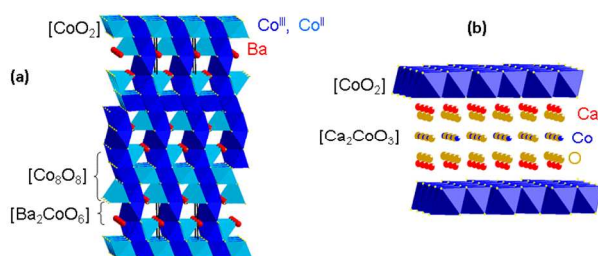


Fig. 1 Crystal structures of (a) Ba₂Co₉O₁₄ and (b) Ca₃Co₄O_{9+ δ}

In contrast, a thermal expansion coefficient of only 10×10^{-6} K⁻¹ was measured for the well-known Ca₃Co₄O_{9+ δ} thermoelectric compound¹² whose structure is a misfit composed of CdI₂-type [CoO₂] layers sandwiched in between [Ca₂CoO_{3- δ}] rock salt slabs^{13,14} (Fig 1b). With an electronic conductivity of 100 S.cm⁻¹ at 700°C and oxygen vacancies in the rock salt layers, Mixed Ionic Electronic Conductivity was expected for this compound. When tested in symmetrical cell with a GDC electrolyte, ASR of 4.94 $\Omega\cdot\text{cm}^2$ for the pure compound and 1 $\Omega\cdot\text{cm}^2$ for a 70 wt% Ca₃Co₄O_{9+ δ} - 30 wt% GDC composite electrode were first measured^{15,16}. After optimisation of composition and thickness it was decreased to 0.5 $\Omega\cdot\text{cm}^2$ at 700°C for a 50 wt% Ca₃Co₄O_{9+ δ} - 50 wt% GDC composite electrode with a thickness of 21 μm , and further decrease to 0.35 $\Omega\cdot\text{cm}^2$ when calcium was partly substituted with 10% of strontium¹⁷. These good performances were confirmed by Samson *et al.*¹⁸, who reported a polarization resistance of 0.64 $\Omega\cdot\text{cm}^2$ at 600°C for a 50 vol% Ca₃Co₄O_{9+ δ} - 50 vol% GDC composite electrode. Using a samarium doped ceria electrolyte, Zou *et al.*¹⁹ measured a maximum power density of 430 mW.cm⁻² at 700°C for a 70 wt% Ca_{2.9}Bi_{0.1}Co₄O_{9+ δ} - 30 wt% Ce_{1.8}Sm_{0.2}O_{1.95} | Ce_{1.8}Sm_{0.2}O_{1.95} | Ce_{1.8}Sm_{0.2}O_{1.95}-Ni button cell.

More recently, oxygen diffusion in this material was confirmed by combing ¹⁸O/¹⁶O isotope exchange, electrical conductivity relaxation and pulse isotopic exchange techniques²⁰. Despite low diffusion with coefficient of 2.7×10^{-10} cm².s⁻¹ at 700°C,

this study showed high kinetics toward oxygen dissociation with a surface exchange coefficient as high as 1.6×10^{-7} cm.s⁻¹. In the present paper, oxygen diffusion in these two innovative cathodes was investigated with an emphasis put on the impact of calcium partial substitution with strontium on the Ca₃Co₄O_{9+ δ} oxygen transport properties.

Experimental

Ba₂Co₉O₁₄ and (Ca_{1-x}Sr_x)₃Co₄O_{9+ δ} (x=0.1, 0.2) powders were prepared by solid-state reaction from the corresponding carbonates and oxides BaCO₃ (Prolabo – 99.5%, dried at 100°C), CaCO₃ (Prolabo – 99.5%, dried at 100°C), SrCO₃ (Aldrich – 99.8%, dried at 100°C) and Co₃O₄ (Alfa Aesar, 99.7%). Reactants were carefully ground in an agate mortar and then calcined repeatedly at 900°C with intermediate grinding. Purity of samples was checked by X-ray diffraction (D8 advance Bruker AXS diffractometer, Cu K α radiation, 1D LynxEye PSD detector). The Fullprof software [v2.05, July 2011] was used for refinement of the unit cell parameters²¹. An Accupyc II 1340 Micromeritics pycnometer was used to measure the powder density. The absolute oxygen stoichiometry of the sample was determined by iodometric titration²².

Thermal analyses were conducted under air, using a TG/DTA Setaram Setsys apparatus. 40 mg of the sample powder was introduced into a Pt crucible, and the experiment was carried out at a heating rate of 5°C/min under flowing air (0.4 L/h) from room temperature to 950°C. A blank experiment with an empty crucible was performed to correct the data for effects of buoyancy. Thermogravimetry was also carried out for evaluation of the oxygen stoichiometry of the sample as a function of pO₂. In this case, a Setaram 92-1750 apparatus was used. The experiment was carried out using 50 mg of powder in a Pt crucible under flowing O₂/N₂ mix (5 L/h), with three successive oxygen partial pressures (100, 200 and 400 mbar), and temperature ranging from 600 to 750°C (50°C step) for each pressure. For this set-up, the buoyancy was negligible and the data were directly used to derive the thermodynamic factor at each temperature.

Dense ceramics, 3 mm thick, were prepared by Spark Plasma Sintering at the IdF Platform in Thiais (France). A 20 mm (diameter) carbon die was used. The samples were sintered within 15 minutes with a 2 minutes dwell at 850°C, under a 50 Mpa (8.8 kN) pressure. To remove carbon residues the pellets were annealed for 12 h at 800°C. A Hitachi S-3400N was used to characterise the samples' surface.

For Isotopic Exchange and Electrochemical Conductivity Relaxation, samples surfaces were roughly polished in a first step before polishing down to 1/4th of micron with successive SiC papers and diamond pastes (Ra~10-20nm) in a second step. In case of calcium cobaltites, to avoid evolution of the surface roughness, samples were annealed for 72 h at 900°C before the second polishing in order to release residual strains in the material.

The $^{18}\text{O}/^{16}\text{O}$ Isotope Exchange Depth Profiling technique was applied to all samples to derive the oxygen self-diffusion tracer (D^* , cm^2/s) and surface exchange coefficients (k^* , cm/s). The diffusion time was chosen to get diffusion lengths significantly smaller than the sample dimensions to consider a 1D diffusion model perpendicular to the surface of the dense ceramic into a semi-infinite medium. In these conditions, assuming first order surface exchange reaction and constant ^{18}O concentration during the exchanges, the solution for a semi-infinite solid to the Fick's 2nd law of diffusion is given by the following equation²³:

$$C'(x, t) = \frac{C(x, t) - C_{bg}}{C_g - C_{bg}} = \text{erfc} \left[\left(\frac{x}{2 \times \sqrt{D^* \times t}} \right) \right] - \left[\exp \left(\frac{k^* x}{D^*} + \frac{k^{*2} t}{D^*} \right) \times \text{erfc} \left(\frac{x}{2 \times \sqrt{D^* \times t}} + k^* \sqrt{\frac{t}{D^*}} \right) \right] \quad [1]$$

where C_{bg} is the natural ^{18}O ratio, C_g the ^{18}O ratio in the enriched exchange atmosphere, x the distance from the surface of the specimen and t the time of the isotope exchange.

Exchange conditions are reported in Table 1. Experiments were carried out in between 650 and 750°C under a pressure close to 210 mbar with a pre-annealing under normal oxygen (search grade oxygen 99.995% ALPHAGAZ) to reach thermodynamic equilibrium prior to the exchange under labelled oxygen. For both annealings, under the ^{18}O enriched atmosphere or pre-annealing, the samples were annealed for the required time, and quenched. To determine the ^{18}O content in the oxygen gas used for the exchange, a silicon wafer was oxidised overnight at 1000°C under 200 mbar.

Table 1. Conditions of $^{18}\text{O}/^{16}\text{O}$ isotope exchange.

Temperature (°C)	Pressure (mbar)	Pre-annealing time (hours)	Annealing time (min)	^{18}O ratio in the gas phase
Ba₂Co₉O₁₄				
648	210	240	2860	0.79
700	210	96	2765	0.80
750	218	96	2790	0.80
(Ca_{1-x}Sr_x)₃Co₄O_{9+δ} x=0.10, 0.20				
604	207	160	725	0.88
649	211	100	567	0.67
694	219	61	392	0.80
741	210	20	55	0.9

A ToF-SIMS⁵ machine (ION-TOF GmbH, 25 keV Bi⁺ LMIG analysis gun, DSCS sputter gun) was used to measure the ^{18}O diffusion profiles using the same experimental protocol as described in ref 20. Both depth analysis from the sample surface (depth profile mode)²⁴ and edge analysis of the cut sample (line scan mode)²⁵ were performed and profiles merged. Depth of craters, after SIMS depth profiling, were measured with a KLA Tencor Alpha-step IQ profilometer. The same apparatus was used to measure the samples' roughness. Electrical Conductivity Relaxation was also carried out on strontium doped Ca₃Co₄O_{9+δ}. For this purpose, plane-parallel

samples (17 mm in length and 1 to 2.4 mm in width) were cut from the strontium substituted dense ceramics using a diamond saw. Electrical conductivity was measured using the 4 points configuration while changing the oxygen concentration of the surrounding atmosphere as shown in ref 20. A gold paste was used to paint gold contacts which were sintered at 750 °C for 1h at a rate of 100 °C/h before experiment. The distance between the two internal electrodes was about 14 mm.

Once the sample was at equilibrium at given temperature, the $p\text{O}_2$ was step-wise changed and the conductivity was monitored as a function of time. The variation of $p\text{O}_2$ was performed by an abrupt switch among air and mixtures of O₂/Ar with oxygen partial pressures of 0.05 atm and 0.01 atm, respectively, at a 5L/h flow rate. In addition, the temperature-dependent electrical conductivity was measured under air with 5L/h flow rate at a very slow speed of 25 °C/h.

To characterise the nature of the atoms at the uppermost surface of the sample, Low-Energy Ion Scattering (LEIS) was also applied to a dense ceramic (Ca_{1-x}Sr_x)₃Co₄O_{9+δ} with x=0.1 composition which had been heated at 800°C in air during 12 hours prior to the analysis. The analysis was performed using a Qtac¹⁰⁰ (ION-TOF GmbH) apparatus. Before analysis, the sample was *in situ* submitted to an atomic oxygen treatment ($2-3 \times 10^{-4}$ mbar) to remove possible organic surface contamination. The study was carried out with a ⁴He⁺ (3keV) beam on a 1mm² analysed area.

Results and discussion

Characterization of powder and ceramics. Synthesised powders and dense ceramics purity was confirmed by X-ray diffraction. As shown in Fig. 2, a good pattern matching was obtained for both type of ceramics.

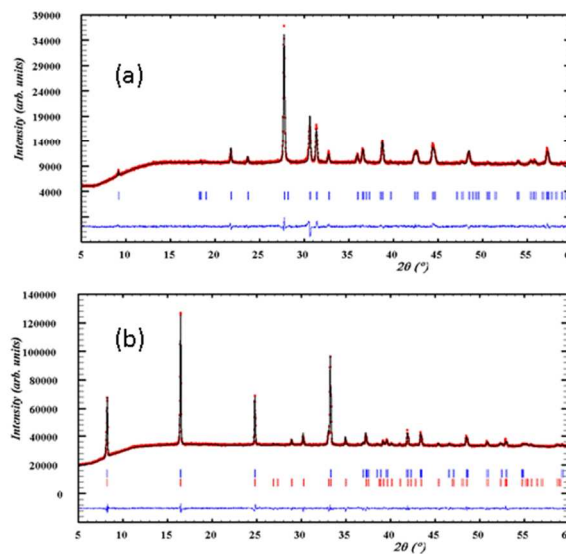


Fig. 2. XRD calculated profile compared to experimental data collected on dense pellets of Ba₂Co₉O₁₄ (a), and (Ca_{1-x}Sr_x)₃Co₄O_{9+δ} with x=0.10 (b).

Corresponding unit-cell parameters are given in Table 2. For $\text{Ba}_2\text{Co}_9\text{O}_{14}$, they are in good agreement with the parameters reported by Ehora *et al.* (5.6963(8) Å, 28.924(6) Å)⁹ and Sun *et al.* (5.6958(4) Å, 28.909(4) Å)¹⁰, the small difference observed between the powders and the ceramics, on one hand, and these authors, on the other hand, being likely due to small difference in the oxygen content due to different thermal histories. For the refinement of $(\text{Ca}_{1-x}\text{Sr}_x)_3\text{Co}_4\text{O}_{9+\delta}$, the phases were considered as a mixture of two phases, one corresponding to the $[\text{CoO}_2]$ layers and the second one corresponding to the $[\text{Ca}_2\text{CoO}_{3-\delta}]$ rock salt layers, with common a , c and β cell parameters, constrained to be the same, and different b_H and b_{RS} , refined independently. The evolution of the unit cell parameters with the strontium content is in good agreement with the results reported by Wang *et al.*²⁶, who showed almost no variation of the b_H unit cell characterising the $[\text{CoO}_2]$ layers periodicity and an increase of the b_{RS} unit cell with strontium content in good agreement with the higher radius of Sr^{2+} (1.18 Å) compared to Ca^{2+} (1.00 Å)²⁷.

Table 2. $\text{Ba}_2\text{Co}_9\text{O}_{14}$ and $(\text{Ca}_{1-x}\text{Sr}_x)_3\text{Co}_4\text{O}_{9+\delta}$ $x=0.1, 0.2$ unit cell parameters from XRD on powder and dense ceramics.

	Powder	Dense ceramics
$\text{Ba}_2\text{Co}_9\text{O}_{14}$ (R $\bar{3}m$)		
a (Å)	5.6945(3)	5.700(1)
b (Å)	28.905(2)	28.926(6)
$(\text{Ca}_{1-x}\text{Sr}_x)_3\text{Co}_4\text{O}_{9+\delta}$ $x=0.10$		
a (Å)	4.8429(3)	4.8433(9)
b_H (Å)	2.8255(3)	2.825(4)
b_{RS} (Å)	4.5968(6)	4.563(2)
c (Å)	10.8730(4)	10.881(2)
β (°)	98.137(9)	98.14(3)
$(\text{Ca}_{1-x}\text{Sr}_x)_3\text{Co}_4\text{O}_{9+\delta}$ $x=0.20$		
a (Å)	4.8518(3)	4.8547(6)
b_H (Å)	2.8225(5)	2.821(1)
b_{RS} (Å)	4.6304(8)	4.6362(8)
c (Å)	10.8995(7)	10.904(2)
β (°)	98.123(7)	98.12(2)

As shown by Ehora *et al.*⁹, $\text{Ba}_2\text{Co}_9\text{O}_{14}$ decomposed into CoO and a cubic BaCoO_2 form at 1030°C. To check the stability of the calcium cobaltites, TGA and DTA analyses were carried out on the two strontium doped compositions. Their thermograms are compared to the signals measured for the non-doped compound in Fig. 3. They exhibit similar behavior. The first transition observed at 130°C for the pure compound disappears when strontium is introduced in the structure, the second transition at 550°C, corresponding to the beginning of a mass loss is maintained at the same temperature but the intensity of the associated endothermic peak on heating decreases with the increase of strontium content. All compounds decomposed before 950°C, the temperature of decomposition being slightly lowered when strontium content increases. This decomposition process is reversible but it is worth noting that the recombination happens at a lower temperature when substitution rate increases.

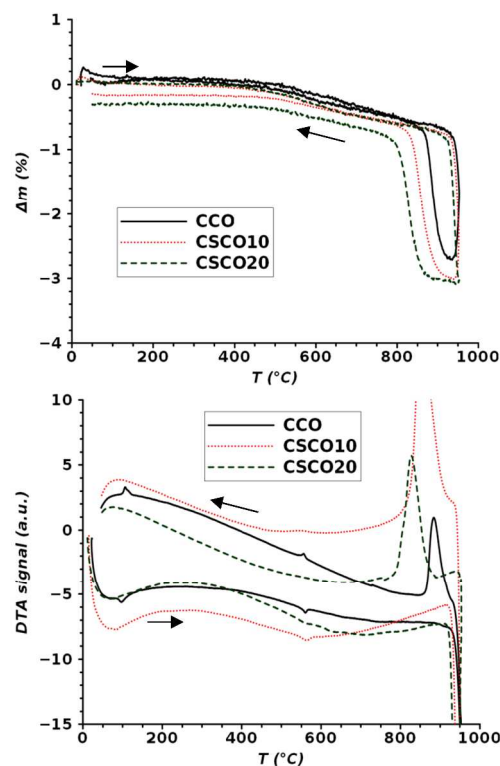


Fig. 3. Comparison of TGA and DTA corresponding to the $\text{Ca}_3\text{Co}_4\text{O}_{9+\delta}$ parent compound (CCO, black solid line), $(\text{Ca}_{1-x}\text{Sr}_x)_3\text{Co}_4\text{O}_{9+\delta}$ with $x=0.10$ (CSCO10, red line) and $(\text{Ca}_{1-x}\text{Sr}_x)_3\text{Co}_4\text{O}_{9+\delta}$ with $x=0.20$ (CSCO20 black dotted line).

Because of lack of stability at high temperature, it was not possible to sinter these compounds by conventional sintering but dense ceramics were obtained by spark plasma sintering with relative densities higher than 96% as confirmed by SEM (see Fig. 4).

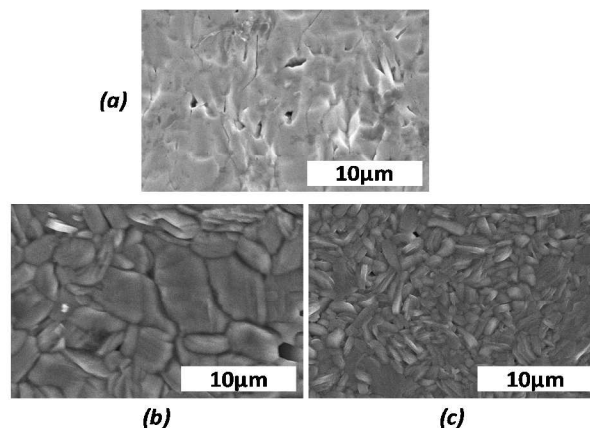


Fig. 4. SEM images of $\text{Ba}_2\text{Co}_9\text{O}_{14}$ (a), and $(\text{Ca}_{1-x}\text{Sr}_x)_3\text{Co}_4\text{O}_{9+\delta}$ with $x=0.10$ (b) and 0.20 (c) showing dense ceramics.

$^{18}\text{O}/^{16}\text{O}$ isotope exchange in $\text{Ba}_2\text{Co}_9\text{O}_{14}$

The normalised $^{18}\text{O}/(^{16}\text{O}+^{18}\text{O})$ isotope concentration in function of penetration depth are given in Fig. 5 for the three studied temperatures. Both data recorded in depth-profile and line-scan mode are reported. A good junction between the two sets of data was

observed. However, whatever the temperature of exchange, a high oxygen content was measured at the surface of the samples in the first microns depth, the thickness of this high oxygen content layer increasing with the temperature. It was therefore not possible to fit these data to the diffusion equation [1].

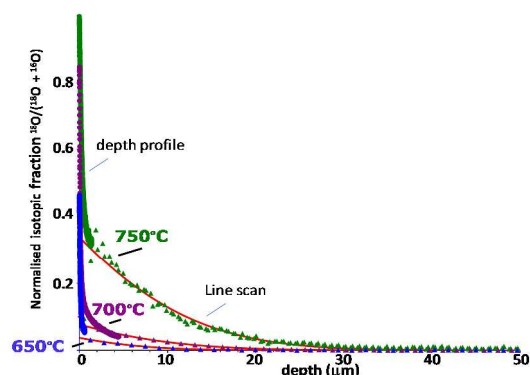


Fig. 5. Normalised ^{18}O diffusion profile measured on $\text{Ba}_2\text{Co}_9\text{O}_{14}$ dense ceramics after annealing under labelled oxygen at 650°C, 700°C and 750°C for about 46 hours and corresponding fit (in red) taking into account the data far from the surface.

Taken into account only the data far from the surface, the transport parameters given in Table 3 were derived.

Table 3. Tentative $\text{Ba}_2\text{Co}_9\text{O}_{14}$ transport parameters derived from normalised ^{18}O isotope profile far from the sample edges.

T (°C)	k^* ($\text{cm}\cdot\text{s}^{-1}$)	D^* ($\text{cm}^2\cdot\text{s}^{-1}$)
648	1.3×10^{-10}	2.5×10^{-12}
700	4.0×10^{-10}	5.0×10^{-12}
750	2.5×10^{-9}	6.0×10^{-12}

Surprisingly, despite very good electrochemical performances, rather low oxygen diffusion and kinetics toward oxygen molecule dissociation were shown. However, one must be careful with these results. The increase of ^{18}O at the sample surface is not clearly understood. It is likely due to an oxidation process when cooling the sample but this hypothesis still has to be confirmed.

Oxygen transport in strontium doped $\text{Ca}_3\text{Co}_4\text{O}_9$

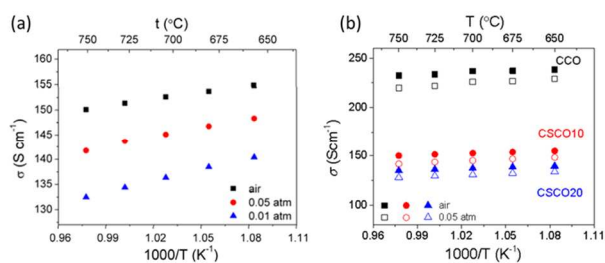


Fig. 6. Evolution of the electrical conductivity of $(\text{Ca}_{1-x}\text{Sr}_x)_3\text{Co}_4\text{O}_{9+\delta}$ with $x=0.10$ composition at thermodynamic equilibrium under different oxygen pressures (a) and comparison of composition $x=0$ (CCO in black), $x=0.10$ (CSCO10 in red) and $x=0.20$ (CSCO20 in blue) electrical conductivities in function of temperature under air and 0.05 atm (b).

The oxygen transport properties in the two strontium doped $\text{Ca}_3\text{Co}_4\text{O}_{9+\delta}$ were characterised by both Electrical Conductivity Relaxation and the $^{18}\text{O}/^{16}\text{O}$ Isotope Depth Profile Technique. The electrical conductivity at thermodynamic equilibrium corresponding to the $x=0.10$ composition under different oxygen pressures is given in Fig. 6a. An increase of the electrical conductivity when the oxygen partial pressure increased was observed, confirming the p-type behaviour of these materials. As shown in Fig. 6b, the electrical conductivity slightly decreased when strontium was introduced in the structure. The evolution of electrical conductivity corresponding to the $(\text{Ca}_{1-x}\text{Sr}_x)_3\text{Co}_4\text{O}_{9+\delta}$ ($x=0.1$) composition at 750°C with surrounding atmosphere changes is shown Fig. 7. It is worth noting that oxidation and reduction are reversible processes.

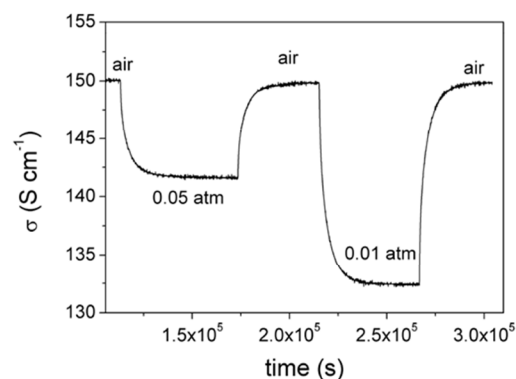


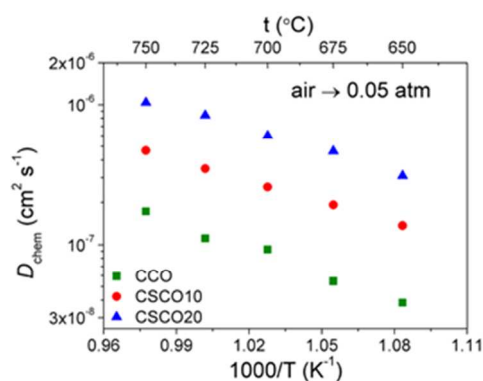
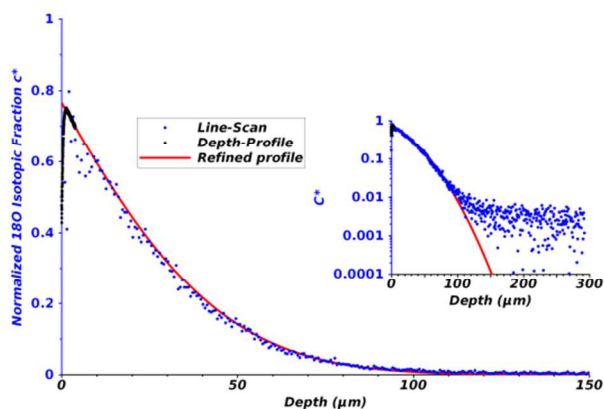
Fig. 7. Evolution of the electrical conductivity of $(\text{Ca}_{1-x}\text{Sr}_x)_3\text{Co}_4\text{O}_{9+\delta}$ with $x=0.10$ composition at 750°C with surrounding atmosphere changes showing the reversibility of oxidation and reduction processes.

Data obtained for both compositions in the 650-750°C range were fitted to the theoretical model of diffusion. In these conditions, only the diffusion coefficient could be derived with precision, reflecting a $D_{\text{chem}}/k_{\text{chem}}$ characteristic length much smaller than the size of the sample and suggesting much higher surface exchange kinetics for these materials than chemical diffusion²⁸. Corresponding D_{chem} values are given in Table 4 shown in Fig. 8. D_{chem} values obtained from the air \leftrightarrow 0.05 atm and air \leftrightarrow 0.01 atm are close and similarly to what was obtained for the pure material²⁰, moreover the chemical diffusion coefficients are independent of whether the relaxation is a reduction or an oxidation process.

As shown in Fig. 8, as expected the diffusion process is thermally activated and activation energies of $1.03\pm 0.03\text{eV}$ and $0.98\pm 0.04\text{eV}$ were measured for the $x=0.1$ and $x=0.2$ compositions, respectively, slightly lower than the activation energy displayed by the pure compound ($1.2\pm 0.02\text{eV}$) indicating easier diffusion for the strontium doped compound which also exhibit higher oxygen diffusion coefficients.

Table 4. D_{chem} ($\text{cm}^2/\text{s}^{-1}$) corresponding to $(\text{Ca}_{1-x}\text{Sr}_x)_3\text{Co}_4\text{O}_{9+\delta}$ with $x=0.1$ and $x=0.2$.

T (°C)	air-0.05 atm	0.05 atm-air	air-0.01 atm	0.01 atm-air
$(\text{Ca}_{1-x}\text{Sr}_x)_3\text{Co}_4\text{O}_{9+\delta}$ $x=0.10$				
650	1.37×10^{-7}	1.35×10^{-7}	1.34×10^{-7}	1.31×10^{-7}
675	1.92×10^{-7}	1.91×10^{-7}	1.85×10^{-7}	1.95×10^{-7}
700	2.58×10^{-7}	2.51×10^{-7}	2.52×10^{-7}	2.57×10^{-7}
725	3.47×10^{-7}	3.61×10^{-7}	3.44×10^{-7}	3.53×10^{-7}
750	4.68×10^{-7}	4.95×10^{-7}	4.73×10^{-7}	4.76×10^{-7}
$(\text{Ca}_{1-x}\text{Sr}_x)_3\text{Co}_4\text{O}_{9+\delta}$ $x=0.20$				
650	3.09×10^{-7}	3.17×10^{-7}	3.04×10^{-7}	3.25×10^{-7}
675	4.62×10^{-7}	4.54×10^{-7}	4.57×10^{-7}	4.58×10^{-7}
700	5.99×10^{-7}	6.40×10^{-7}	5.87×10^{-7}	6.37×10^{-7}
725	8.41×10^{-7}	8.50×10^{-7}	8.00×10^{-7}	8.24×10^{-7}
750	1.04×10^{-6}	1.14×10^{-6}	0.96×10^{-6}	1.08×10^{-6}

Fig. 8. Evolution of D_{chem} as a function of temperature measured on the parent compound $\text{Ca}_3\text{Co}_4\text{O}_{9+\delta}$ (CCO, green square), $(\text{Ca}_{1-x}\text{Sr}_x)_3\text{Co}_4\text{O}_{9+\delta}$ with $x=0.10$ (CSCO10, red dot) and $x=0.20$ (CSCO20 blue triangle).Fig. 9. Normalised ^{18}O diffusion profile measured on the $(\text{Ca}_{1-x}\text{Sr}_x)_3\text{Co}_4\text{O}_{9+\delta}$ $x=0.1$ composition, exchanged at 649°C during 567 minutes under 211 mbar dry oxygen. Calculated profile is given in red.

This increase of oxygen diffusion coefficient with substitution ratio was confirmed by $^{18}\text{O}/^{16}\text{O}$ isotope exchange. The normalized ^{18}O diffusion profile corresponding to the $(\text{Ca}_{1-x}\text{Sr}_x)_3\text{Co}_4\text{O}_{9+\delta}$ with $x=0.1$ composition, exchanged at 649°C during 567 minutes under 211 mbar dry oxygen is shown in Fig. 9. Again a good junction was

obtained between data collected in depth profile mode and line scan mode.

However in this case, as shown for the parent compound²⁰, a small decrease of the ^{18}O content was noticed at the sample surface, attributed to a possible carbonation or hydroxylation when back to ambient atmosphere. In insert, the same plot in decimal logarithm scale has been drawn to compare experimental and theoretical profiles far in depth. As previously noticed for the pure compound, a «tail» can be seen, suggesting most likely an anisotropic diffusion²⁰. Nevertheless, as shown in Fig. 9, a good fit between the calculated and experimental data was obtained. The derived k^* and D^* parameters are given in Table 5. Their evolution as a function of temperature is given on an Arrhenius plot in Fig. 10.

Table 5. D^* ($\text{cm}^2/\text{s}^{-1}$) and k^* (cm/s^{-1}) corresponding to $(\text{Ca}_{1-x}\text{Sr}_x)_3\text{Co}_4\text{O}_{9+\delta}$ with $x=0.1$ and $x=0.2$.

T (°C)	604	649	694	741
$(\text{Ca}_{1-x}\text{Sr}_x)_3\text{Co}_4\text{O}_{9+\delta}$ $x=0.10$				
k^*	1.4×10^{-8}	1.9×10^{-7}	3.0×10^{-6}	3.0×10^{-6}
D^*	1.1×10^{-10}	2.5×10^{-10}	4.1×10^{-10}	1.0×10^{-9}
$(\text{Ca}_{1-x}\text{Sr}_x)_3\text{Co}_4\text{O}_{9+\delta}$ $x=0.20$				
k^*	6.7×10^{-8}	3.0×10^{-7}	4.0×10^{-6}	2.0×10^{-6}
D^*	3.0×10^{-10}	2.8×10^{-10}	6.1×10^{-10}	6.7×10^{-10}

The tracer diffusion can be correlated to chemical diffusion via the thermodynamic factor γ according to the following equation.

$$D_{\text{chem}} = \gamma D^*$$

$$\gamma = 1/2 \cdot \frac{\Delta \ln p_{\text{O}_2}}{\Delta \ln c_{\text{O}}} \approx 1/2 \cdot \frac{\Delta \ln p_{\text{O}_2}}{\Delta \ln c_{\text{O}}} \text{ when } \sigma_e \gg \sigma_i \quad [2]$$

where $\Delta \ln p_{\text{O}_2}$ and $\Delta \ln c_{\text{O}}$ are the corresponding variations in the oxygen partial pressure and oxygen content, and σ_e and σ_i are the electronic and ionic conductivity, respectively.

For sake of comparison, the evolution of $D_{\text{ECR}}^* = D_{\text{chem}}^*/\gamma$ is also reported in Fig. 10. Values are in good agreement. The slightly higher values observed for D_{ECR}^* compared to the tracer diffusion coefficient values can be explained by a lack of accuracy in the determination of the thermodynamic coefficient because of small oxygen stoichiometry variations (see value of the thermodynamic coefficient in Table 6).

Table 6. $(\text{Ca}_{1-x}\text{Sr}_x)_3\text{Co}_4\text{O}_{9+\delta}$ ($x=0.1$, $x=0.2$) thermodynamic coefficient derived from TGA analysis as a function of temperature and oxygen partial pressure.

Temp. (°C)	$x=0.1$	$x=0.2$
650	211	313
675	200	305
700	189	297
725	183	299
750	178	302

An increase of the diffusion coefficient with the strontium content is confirmed and may be explained by the increase of the rock salt layers volume which may facilitate the oxygen

mobility within these layers. However, with a value in the range of 10^{-10} $\text{cm}^2\cdot\text{s}^{-1}$ it is still low which justify the addition of gadolinia doped ceria to improve electrochemical performances¹⁵⁻¹⁹.

With surface exchange coefficient of 3.0×10^{-6} $\text{cm}\cdot\text{s}^{-1}$ and 4.0×10^{-6} $\text{cm}\cdot\text{s}^{-1}$ at 700°C for both $x=0.1$ and $x=0.2$ compositions, these materials exhibit very fast kinetics for the oxygen reduction reaction compared to the best cathode materials in the field since values of only 1.3×10^{-7} , 1.1×10^{-6} and 1.3×10^{-7} were reported for $\text{La}_2\text{NiO}_{4+\delta}$ at 700°C ²⁹, $\text{La}_{0.6}\text{Sr}_{0.4}\text{CoO}_{3-\delta}$ at 680°C ⁴ and $\text{GdBaCo}_2\text{O}_{5+\delta}$ at 686°C ³⁰, respectively.

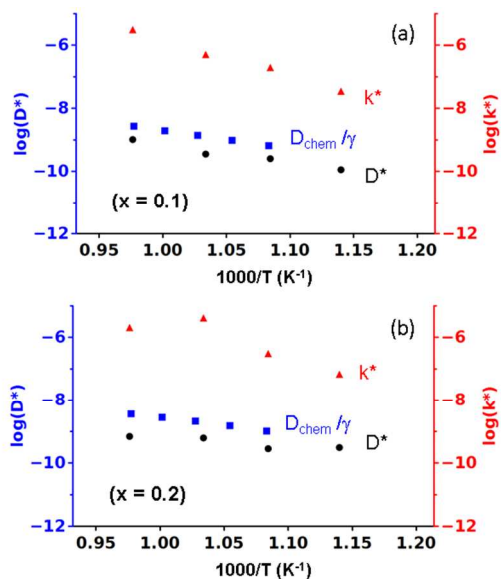


Fig. 10. Arrhenius plot of k^* and D^* compared to D_{chem}/γ for composition $(\text{Ca}_{1-x}\text{Sr}_x)_3\text{Co}_4\text{O}_{9+\delta}$ with $x=0.1$ (a) and $x=0.2$ (b).

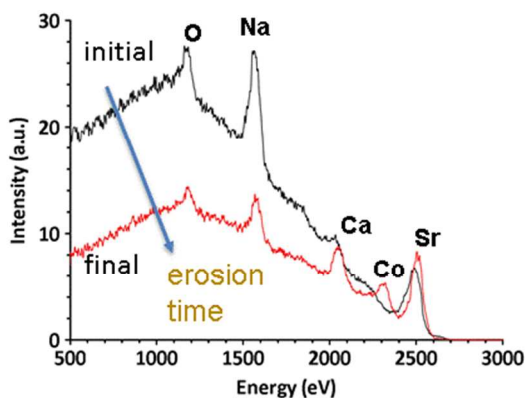


Fig. 11. $^4\text{He}^+$ (3keV) LEIS spectra recorded on a dense ceramics of $(\text{Ca}_{1-x}\text{Sr}_x)_3\text{Co}_4\text{O}_{9+\delta}$ with $x=0.1$ after annealing at 800°C for 12 hours prior to the analysis. The first spectrum (in black) corresponds to an estimated removal of 0.2 monolayer and the last spectrum (in red) to an expected removal of around 3 monolayers.

To go further in the understanding of oxygen transport in these materials, the $x=0.1$ composition was characterised by LEIS. The

initial spectrum corresponding to an estimated removal of 0.2 monolayer is compared to the one measured after an estimated removal of 3 monolayers in Fig. 11. Despite a bulk contamination with sodium which was also observed at the surface of powders and ceramics of the parent compound²⁰, mainly strontium and calcium were initially observed at the uppermost sample surface. No cobalt was initially observed, just a sub-surface signal at low energy side from the surface peak³¹ in the background indicating cobalt atoms are beneath the first measured atomic layer. After ionic sputtering, cobalt was evidenced at the outermost surface and an increase of calcium was also noticed. Although, one must be careful with this technique since strontium may also segregate at the sample surface, the same behaviour was observed for other compounds. For SmCoO_3 , Fullarton *et al.* also showed that samarium was preferentially at the surface with only 5% of cobalt at the outmost surface and a segregation of strontium at the surface was evidenced for strontium doped compounds³². Similarly, Viitanen *et al.* showed the absence of cobalt and iron in the outermost atomic layer of a $\text{La}_{0.6}\text{Sr}_{0.4}\text{Co}_{0.2}\text{Fe}_{0.8}\text{O}_3$ membrane³³. We also showed calcium oxide at the uppermost surface of the $\text{Ca}_3\text{Co}_4\text{O}_9$ parent compound. Here, strontium seems to be mainly at the sample surface and its presence may partly explain the increase of kinetics towards the oxygen dissociation reaction when strontium content increases.

Conclusions

Although oxygen diffusion was confirmed in the promising $\text{Ba}_2\text{Co}_9\text{O}_{14}$, it was not possible to derive accurate transport parameters because of an oxidation process at the sample surface which has still to be clarified. In contrast, for $\text{Ca}_3\text{Co}_4\text{O}_{9+\delta}$ derivatives, it was shown that oxygen diffusion was improved when calcium was partly substituted with strontium likely due to an increase of the volume of the rock salt layers of the structure which may help for oxygen mobility. Although diffusion coefficient remains low, interestingly fast kinetics towards oxygen dissociation reaction were shown with surface exchange coefficient higher than those reported for the best cathode materials in the field. The surface exchange coefficient is increased when the strontium content increases which may be correlated to the presence of a higher amount of strontium at the sample surface which may play a key role in the mechanism of the oxygen molecule dissociation at the surface of the solid.

Acknowledgments

The "Fonds Européen de Développement Régional (FEDER)", "CNRS", "Région Nord Pas-de-Calais" and French "Ministère de l'Education Nationale de l'Enseignement Supérieur et de la Recherche" are acknowledged for funding of X-ray and surface analyses facilities. V.T. is grateful to the University Lille 1 for funding his PhD grant. The authors are also grateful to the Agence Nationale de la Recherche for funding the ANR EVEREST (ANR-07-PANH-005), NanOxyDesign (ANR-10-BLAN-0814) and IDEA-MAT (ANR-12-BS08-0012-01) projects.

Maxence Vandewalle, Nora Djelal and Laurence Burylo from UCCS are acknowledged for SEM, TG-DTA analyses and conventional XRD experiments, respectively.

Notes

^a Laboratoire Structures, Propriétés et Modélisation des Solides (SPMS), Ecole Centrale Paris, Grande Voie des Vignes, 92295 Châtenay-Malabry, France

^b Univ Lille Nord de France, CNRS UMR 8181, Unité de Catalyse et de Chimie du Solide - UCCS, ENSCL, Université Lille 1, CS 90108, 59652 Villeneuve d'Ascq Cedex, France

*corresponding author, email: rose-noelle.vannier@ensc-lille.fr, Tel +33(0)320436583, Fax +33(0)320436814

References

- Functional materials for sustainable energy applications, Woodhead publishing series in energy, edited by John A. Kilner, Stephen J. Skinner, Stuart J.C. Irvine, Peter P. Edwards, Woodhead Publishing Limited, 2012.
- D. Marinha, J. Hayd, L. Dessemond, E. Evers-Tiffée, E. Djurado, *J. Power Sources*, 2011, **196**, 5084.
- Y. Li, M.W. Xu, J.B. Goodenough, *J. Power Sources*, 2012, **209**, 40.
- A.V. Berenov, A. Atkinson, J.A. Kilner, E. Bucher, W. Sitte, *Solid State Ionics*, 2010, **181**, 819.
- O. Yamamoto, *Electrochimica Acta*, 2000, **45**, 2423.
- K. Kordesch, G. Simader, *Fuel Cells and their Applications*, VCH, Weinheim/Wiley, NY, 1996.
- B. Fan, J. Yan, X. Yan, *Solid State Sciences*, 2011, **13**, 1835.
- A. Rolle, N. Preux, G. Ehora, O. Mentré, S. Daviero-Minaud, *Solid State Ionics*, 2011, **184**, 31.
- G. Ehora, S. Daviero-Minaud, M. Colmont, G. André, O. Mentré, *Chem. Mater.*, 2007, **19**, 2180.
- J. Sun, M.; Yang, G. Li, T. Yang, F. Liao, Y. Wang, M. Xiong, J. Lin, *Inorg. Chem.*, 2006, **45**, 9151.
- I. Kehal, to be published
- K. Nagasawa, S. Daviero-Minaud, N. Preux, A. Rolle, P. Roussel, H. Nakatsugawa, O. Mentré, *Chem. Mater.*, 2009, **21**, 4738.
- H. Muguerra, D. Grebille, F. Bourée, *Acta Cryst.*, 2008, **B64**, 676.
- C.D. Ling, K. Aivazian, S. Schmid, P. Jensen, *J. of Solid State Chemistry*, 2007, **180**, 1446.
- Rolle, A.; Boulfrad, S.; Nagasawa, K.; Nakatsugawa, H.; Mentré, O.; Irvine, J.; Daviero-Minaud, S. *J. Power Sources* 2011, **196**, 7328.
- A. Rolle, V. Thoréton, P. Rozier, E. Capoen, O. Mentré, B. Boukamp, S. Daviero-Minaud, *Fuel Cells*, 2012, **12(2)**, 288.
- A. Rolle to be published.
- A.J. Samson, M. Sogaard, N. Van Nong, N. Pryds, N.J. Bonanos, *J. Power Sources*, 2011, **196**, 10606.
- J. Zou, J. Park, H. Yoon, T. Kim, J. Chung, *J. International Journal of Hydrogen Energy*, 2012, **37**, 8592.
- V. Thoréton, Y. Hu, C. Pirovano, E. Capoen, N. Nuns, A.-S. Mamede, G. Dezanneau, C.Y. Yoo, H.J.M. Bouwmeester, R.N. Vannier, *J. Mater. Chem. A*, to be published.
- J. Rodriguez-Carvajal, *Physica B.*, 1993, **192**, 55.
- L. Karvonen, H. Yamauchi, M. Karppinen, *Chem. Mater.*, 2008, **20**, 7143.
- J. Crank, *The Mathematics of diffusion*, 2nd ed. Clarendon Press, Oxford, 1975.
- J.A. Kilner, B.C.H. Steele, L. Ilkov, *Solid State Ionics*, 1984, **12**, 89.
- R.J. Chater, S. Carter, J.A. Kilner, B.C.H. Steele, *Solid State Ionics*, 1992, **53-56**, 859.
- L.B. Wang, A. Maignan, D. Pelloquin, S. Hébert, B. Raveau, *J. Applied Physics*, 2002, **92**, 124.
- R.D. Shannon, *Acta Cryst.*, 1976, **A32**, 751.
- M.W. den Otter, H.J.M. Bouwmeester, B.A. Boukamp, H. Verweij, *J. Electrochem. Soc.*, 2001, **148(2)**, J1.
- R. Sayers, R.A. De Souza, J.A. Kilner, S.J. Skinner, *Solid State Ionics*, 2010, **181**, 386.
- A. Tarancón, S.J. Skinner, R.J. Chater, F. Hernández-Ramirez, J.A. Kilner, *J. Mater. Chem.*, 2007, **17**, 3175.
- H.R.J. ter Veen, T. Kim, I.E. Wachs, H.H. Brongersma, *Catalysis Today*, 2009, **140**, 197.
- I.C. Fullarton, J.P. Jacobs, H.E. Benthem, J.A. Kilner, H.H. Brongersma, P.J. Scanlon, B.C.H. Steele, *Ionics*, 1995, **1**, 51.
- M.M. Viitanen, R.G. Welzenis, H.H. Brongersma, F.P.F. van Berkel, F.P.F., *Solid State Ionics*, 2002, **150**, 223.